Powder Technology 376 (2020) 60–71

Contents lists available at ScienceDirect

Powder Technology

journal homepage: www.elsevier.com/locate/powtec

Uniform shape elongation effects on the random packings of uniaxially variable superellipsoids

Lufeng Liu [a,b], Shuixiang Li [b,*]

[a] Institute of Applied Physics and Computational Mathematics, Beijing, 100094, China
[b] Department of Mechanics and Engineering Science, College of Engineering, Peking University, Beijing, 100871, China

ARTICLE INFO

Article history:
Received 26 June 2020
Received in revised form 4 August 2020
Accepted 6 August 2020
Available online 11 August 2020

Keywords:
Effective aspect ratio
Maximally dense random packing
Uniaxially variable superellipsoid

ABSTRACT

Uniaxially variable (rod-like) particles are common in nature and industry. However, the aspect ratio effects on the random packings for differently shaped rod-like particles are not uniform by their innate definitions of aspect ratios. In this work, we propose new definitions of effective aspect ratios that take the surface shape information into account and observe uniform shape elongation effects on the random packing densities. The packing density reaches a maximal value with the effective aspect ratio to be about 1.5. We also observe symmetric high-density regions on the packing-density map. Finally, we carry out the Voronoi analysis and find that the surface shape of particles plays a more important role in changing the local packing properties than the aspect ratio. Our work provides a uniform definition for the aspect ratio of differently shaped rod-like particles and leads to a better understanding towards the particle shape effects on random packings.

© 2020 Elsevier B.V. All rights reserved.

1. Introduction

The packings of differently shaped particles are widely used to characterize the complex phenomena in liquids, crystals, glasses, colloids, and granular materials. Particle shapes have a significant influence on the phase behaviors and self-assemblies of particles, as well as the packing and mechanical properties of particle systems [1–8]. Packing density, defined as the ratio of the volume of all particles to that of the container, is a common and important parameter in describing random packing systems. Researchers have been pursuing general relations between the packing density of random packings and the shapes of particles for decades.

In recent years, a number of methods and theories have been developed to describe and predict the packing properties (especially the packing density) of random packings with differently shaped particles or polydisperse packings. A "granocentric" model [9], which captured the packing properties ranging from the microscopic distributions of nearest neighbors and contacts to local density fluctuations and then to the global packing density, was devised and successfully used to estimate the global packing density of binary sphere packing systems. Via the analysis of the contact angle distributions, Tian et al. [10] found a universal organizing principle for the maximally random jammed (MRJ) packings of binary frictionless superdisks independent of the detailed particle shape and derived a highly accurate formula for the MRJ densities. Schaller et al. [11] found that the global average contact number was a monotonically increasing function of the global packing density in the frictional ellipsoid packings, which was explained via a local analysis of the Voronoi tessellation. They also found that the standard deviations of the local volume fraction distribution depended only on the global packing density. Kallus [12] estimated the random packing densities for all sufficiently spherical shapes via a fully analytic calculation and he found that all sufficiently spherical shapes packed more densely than spheres. A mean-field theory based on Edwards' ensemble and random first-order glass transition has also been developed to demonstrate the phase diagram of jammed sphere packings and to predict the packing densities of high dimensional or binary sphere packings [3,13].

Elongating or compressing the particles, i.e. changing the aspect ratio of the particles, is a common method to change the structural properties of particle assemblies. The particles elongated or compressed in a single direction are usually called uniaxially variable particles, which are common in nature and industry. For simplicity, the uniaxially variable particle is also noted as the rod-like particle in this work, while the uniaxially variable particle is a more accurate description. The aspect ratio w is usually defined as $w = D/L$, where D is the characteristic length on the cross-section, and L is the characteristic length along the elongating or compressing direction. The aspect ratio effects on the random packing densities of differently shaped rod-like particles were widely studied. The optimal w, where the maximal random packing density was obtained, was about 0.7 or 1.5 for spheroids [14–17], 1.5 for spherocylinders [16,18–26], 0.67 for lens-shaped particles [27], and 1.4 for dimmers [28], as discussed in many simulation results. Recently, Baule et al. [29] applied the mean-field theory to estimate the random

* Corresponding author.
E-mail address: lsx@pku.edu.cn (S. Li).

https://doi.org/10.1016/j.powtec.2020.08.017
0032-5910/© 2020 Elsevier B.V. All rights reserved.

packing densities of axisymmetric non-spherical particles with different aspect ratios based on the Voronoi volumes. In their results, the optimal w for lens-shaped particles was 0.8 and both the optimal w for spherocylinders and dimmers were 1.3. Their predicted results about the locations of the maximal packing density were close to the literature results discussed above. However, the optimal aspect ratios for differently shaped rod-like particles are not uniform under their innate definitions of aspect ratio. In other words, is it possible to find a unique optimal aspect ratio for differently shaped rod-like particles under a special definition of aspect ratio? Meanwhile, the aspect ratio effects on the random packing density of some rod-like particles are still controversial due to different definitions of the random state. Therefore, a common definition of the aspect ratio for differently shaped rod-like particles is needed to understand the aspect ratio effects on the random packing densities under a common random state.

Moreover, we found in recent works that universal shape elongation and compression effects on the random packing densities of the maximally dense random packings (MDRPs) [26,30,31] for symmetric particles with three equivalent axes when $w = 1.0$, such as the spherocylinders [26], spheroids [30], cuboids [31] and the superellipsoids which are elongated or compressed superballs [30]. The maximally dense random packing (MDRP) is defined as the densest packing in the random state in which the particle positions and orientations are randomly distributed [26,30–34]. The packing density of the MDRP corresponds to a sharp transition in the order map, which characterizes the onset of nontrivial spatial correlations among the particles. Therefore, the MDRP state provides a good platform for the comparison of random packing densities of differently shaped particles because all the packings are on the same degree of randomness and the influences of the order are eliminated. The difference in packing densities on the MDRP state is only caused by the variation of particle shape. For all the symmetric particles with three equivalent axes, the packing density versus aspect ratio curves are in "M" type with one minimum at $w = 1.0$ and two maximums at $w \approx 0.7, 1.5$, when all the packings are on the MDRP state [26,30,31]. We also found uniform shape elongation effects for the bi-axially elongated superballs [34] with the ratios of three main axes to be $1 : \alpha^{\beta} : \alpha$. We note that all the particles mentioned above are symmetric particles with three equivalent axes, and the packing density curve of cylinders, which are not axially equivalent, was single-peaked with the maximal packing density obtained when the scaled aspect ratio was about 1.5 as well [32]. Therefore, a uniform shape elongation effect for all rod-like particles, with or without three equivalent axes, seems to be emerged according to our recent results. However, this suggestion needs to be further verified for more non-axially-equivalent particles, which is the main purpose of this work.

In this work, we will investigate the aspect ratio effects on the random packing densities for more general rod-like particles with non-equivalent axes. The rod-like particles with different surface shapes are described via the superellipsoid model, containing the z-dominant and y-dominant superellipsoids, whose random packings are still not well investigated according to our knowledge. We propose new definitions of effective aspect ratios that take the surface shape information into account and observe uniform shape elongation effects on the random packing densities. We obtained the MDRPs of the uniaxially variable superellipsoids via the inverse Monte Carlo (IMC) method [31], which ensures the final packings to be highly disordered. For all the superellipsoids we study, the packing density reaches a maximal value with the effective aspect ratio R to be about 1.5. Moreover, for the y-dominant superellipsoids, of which at least one cross-section changes form a disk to an ellipse, the packing density curves are in "M" shaped with two maximums located at $R \approx 0.7$ and 1.5 and the packing density at $R = 1.0$ is a local minimum. We also study the surface shape effects on the random packing density and symmetric high-density regions are observed on the packing density map. Finally, we calculate the sphericities of the superellipsoids and carry out the Voronoi analysis for all the random packings we generate in this work.

The rest of this paper is organized as follows: In section 2, we introduce the particle models, shape parameters, the packing algorithms, and order parameters. The results and discussion are demonstrated in section 3 and the concluding remarks are given in section 4.

2. Methodology

In this part, we introduce the particle models we use and the effective aspect ratios we define in this work. Then the packing algorithms and order parameters are presented.

2.1. The particle models

The original superellipsoid model introduced by Barr [35] is a rich geometric model and its surface function in the local Cartesian coordinates is defined as

$$\left[\left(\left|\frac{x}{a}\right|\right)^{2p_0} + \left(\left|\frac{y}{b}\right|\right)^{2p_0}\right]^{\frac{p_1}{p_0}} + \left(\left|\frac{z}{c}\right|\right)^{2p_1} = 1.0, \tag{1}$$

where a, b and c are the semi-major axis lengths in the direction of x, y, and z axes, respectively, and can be used to describe the aspect ratio effects. The p_0 and p_1 are the surface shape parameters that determine the sharpness of particles. Here we use the Perram and Wertheim (PW) potential [36–38] to detect whether two superellipsoids are overlapped or not. The superellipsoid model has the ability to represent many common shaped particles and the shape effects on the random packings, densest packings and phase behaviors of some special superellipsoids have been well studied, such as the ellipsoids ($p_0 = p_1 = 1.0$) [14–17,39–48], superballs ($p_0 = p_1 = p$, $a = b = c$) [36,49–51], superellipsoids which are elongated or compressed superballs ($p_0 = p_1 = p, a = b, c = wa$) [30,52,53], and the bi-axially elongated superballs ($p_0 = p_1 = p, a : b : c = 1 : \alpha^{\beta} : \alpha$) [34]. More details about the superellipsoid model and the overlap detection algorithm can be found in Ref. 30.

In this work, we investigate the random packing properties of superellipsoids with the surface parameters $p_0 = 1.0$, $p_1 = p$. These superellipsoids are elongated or compressed in the z or y direction and are not fully axially equivalent. When the superellipsoids are elongated or compressed in the z direction, which is the symmetric axis, the surface function in Eq. (1) degenerates to

$$\left[(|x|)^2 + (|y|)^2\right]^p + \left(\left|\frac{z}{w}\right|\right)^{2p} = 1.0, \tag{2}$$

with $a = b = 1$, $c = w$. The xy plane, which is the main cross-section that perpendicular to the z direction, is always a unit disk, making the superellipsoids to be axisymmetric in the z direction. The xz and yz planes along the z direction are superellipses with the aspect ratio w and the shape parameter p. Here w is the natural aspect ratio in the z direction, which is used to describe the aspect ratio effects. Fig. 1 shows some examples of superellipsoids that are elongated or compressed in the z direction. The surface shape parameter p ranges from 0.7 to 5.0 with the natural aspect ratio w varies from 0.5 to 2.0. As can be seen in Fig. 1, the particle is close to an ideal cylinder when p approaches infinity and close to a bicone when p approaches 0.5. Meanwhile, the superellipsoids are compressed in the z direction if w is smaller than 1.0 and are elongated if w is larger than 1.0. When the aspect ratio w varies from 1.0, both the two cross-sections along the z direction are changing from a superdisk to a superellipse. In this work, we note the superellipsoids defined by Eq. (2) as z-dominant superellipsoids.

Similarly, when the superellipsoids are elongated or compressed in the y direction, which is not the symmetric axis, the surface function in Eq. (1) degenerates to

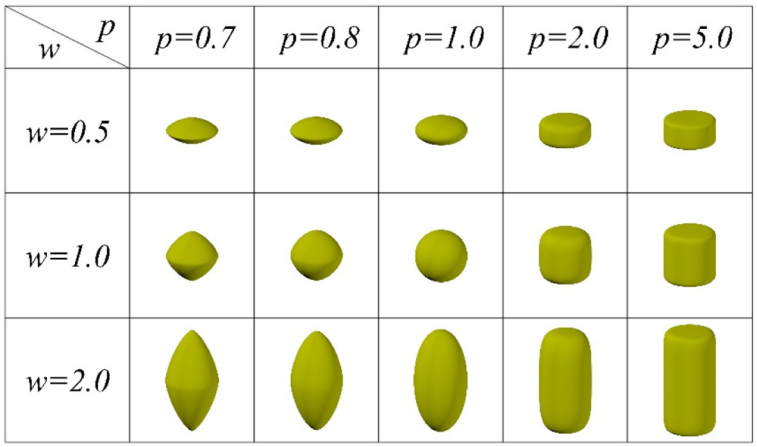

Fig. 1. Some examples of the *z*-dominant superellipsoids defined in Eq. (2) with different surface shape parameter *p* and natural aspect ratio *w*. The superellipsoids are compressed or elongated in the *z* direction.

$$\left[(|x|)^2+\left(\left|\frac{y}{u}\right|\right)^2\right]^p+(|z|)^{2p}=1.0, \tag{3}$$

with $a=c=1, b=u$. Fig. 2 shows some examples of superellipsoids that are elongated or compressed in the *y* direction. The main cross-section perpendicular to the *y* direction becomes the *xz* plane, which is always a superdisk with the shape parameter *p*. The *xy* and *yz* planes along the *y* direction are ellipse and superellipse, respectively. When the aspect ratio *u* varies from 1.0, the *xy* and *yz* planes along the *y* direction are changing from a disk to an ellipse and from a superdisk to a superellipse, respectively, breaking the axial symmetry of the superellipsoids. In this work, we note the superellipsoids defined by Eq. (3) as *y*-dominant superellipsoids. According to our knowledge, both the packing properties of the *z*-dominant and *y*-dominant superellipsoids are still not well investigated.

2.2. The effective aspect ratios

In this work, we propose the definition of the effective aspect ratio for superellipsoids with different surface shapes defined in Eq. (1). For a superellipsoid defined with the three semi-major axis lengths to be *a*, *b* and *c*, the natural aspect ratio can be represented as

$$u=\frac{b}{a}, w=\frac{c}{a}, \tag{4}$$

where *u* and *w* represent the natural aspect ratio in the *y* and *z* direction, respectively. However, for the *z*-dominant superellipsoids studied in this work, the natural aspect ratio is not a good and uniform definition for describing the aspect ratio effects on the random packings of these particles, as can be seen in Fig. 6(a). Therefore, we introduce a new definition of the aspect ratio.

Considering that the shapes of *xy*, *xz* and *yz* planes are not the same for a general superellipsoid with a ≠ b ≠ c, we first define the dimensionless effective axial length L_x, L_y, L_z in three main axial directions,

$$L_x=\left(\frac{S_{xy}\cdot S_{xz}}{S_{yz}^2}\right)^{1/3}, L_y=\left(\frac{S_{xy}\cdot S_{yz}}{S_{xz}^2}\right)^{1/3}, L_z=\left(\frac{S_{xz}\cdot S_{yz}}{S_{xy}^2}\right)^{1/3}. \tag{5}$$

where S_{xy}, S_{xz} and S_{yz} are the areas of the *xy*, *xz* and *yz* planes for a superellipsoid with the surface shape parameters p_0 and p_1, i.e.

$$S_{xy}=abS_0(p_0), S_{xz}=acS_0(p_1), S_{yz}=bcS_0(p_1). \tag{6}$$

where $S_0(p)$ is the area of a unit superdisk with the surface shape parameter *p*,

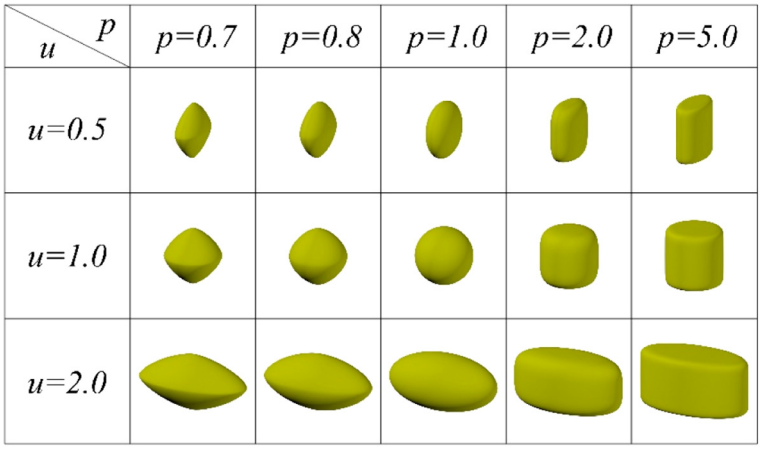

Fig. 2. Some examples of the *y*-dominant superellipsoids defined in Eq. (3) with different surface shape parameter *p* and natural aspect ratio *u*. The superellipsoids are compressed or elongated in the *y* direction.

$$S_0(p) = \frac{\left[\Gamma\left(\frac{1}{2p}\right)\right]^2}{p\Gamma\left(\frac{1}{p}\right)}, \tag{7}$$

with $\Gamma(x) = \int_0^{+\infty} t^{x-1}e^{-t}dt, x > 0$ to be the gamma function.

Therefore, the ratios of the three dimensionless effective axial lengths are $L_x : L_y : L_z = 1 : R_y : R_z$, where R_y and R_z are the effective aspect ratio for the general superellipsoids defined in Eq. (1) and can be used to describe the aspect ratio effects for superellipsoids. The R_y and R_z can be calculated as

$$R_y = \frac{L_y}{L_x} = \frac{S_{yz}}{S_{xz}} = \frac{b}{a} = u, \tag{8}$$

$$R_z = \frac{L_z}{L_x} = \frac{S_{yz}}{S_{xy}} = \frac{cS_0(p_1)}{aS_0(p_0)} = C_s\frac{c}{a} = C_s w. \tag{9}$$

where C_s is the scaling coefficient, which depends only on the surface shape parameters of the superellipsoids and can be defined as

$$C_s = \frac{S_0(p_1)}{S_0(p_0)}. \tag{10}$$

As can be seen from Eqs. (8) and (9), the effective aspect ratio R_y in the y direction is always equal to the natural aspect ratio u, while the effective aspect ratio R_z in the z direction is proportional to the natural aspect ratio w with the scaling coefficient C_s. In this work, for the superellipsoids defined in Eqs. (2) and (3), the scaling coefficient C_s increases with the increase of the surface shape parameter p, as can be seen in Fig. 3. The C_s is equal to the unit when the surface shape parameter $p = 1.0$. For the z-dominant superellipsoids defined in Eq. (2), only the z direction is elongated (compressed) and the effective aspect ratios are $R_y = 1.0$, $R_z = C_s w$. For the y-dominant superellipsoids defined in Eq. (3), only the y direction is elongated (compressed) and the effective aspect ratios are $R_y = u$, $R_z = C_s$.

2.3. The packing algorithms and order parameters

In this work, we generate the random packings of superellipsoids via the inverse Monte Carlo (IMC) method [31], which ensures the final packings to be highly disordered. The IMC method is a Monte Carlo compression process in which the formation of the locally ordered structures can be controlled via order constraints, and is an efficient method to generate packing configurations with a certain degree of order [30–32]. The order constraints are carried out via evaluating some normalized local order parameters Op after each random attempt of a particle moving or boundary deformation. Besides the non-overlapping condition, if the order parameters are larger than a prescribed value Op^{up}, the attempt of particle moving or boundary deformation is also rejected. In this work, the order constraint $Op^{up} = 0.5$, which is a very small value and ensures the final packing to be highly disordered. The configuration is compressed slowly with the compressing rate, which is the reciprocal of the number of particle moves between two boundary deformations, set to be 0.001. The final packing is maximally dense under the order constraints and can be regarded as close approximations to the ideal MDRPs [30–32]. The total number of particles in the packing system is $N = 200$, which is large enough to ignore the system size effect under periodical boundary conditions in all three directions [30–32]. The data demonstrated below are averaged over 5 times and the error bars on the packing density curves are the standard deviations.

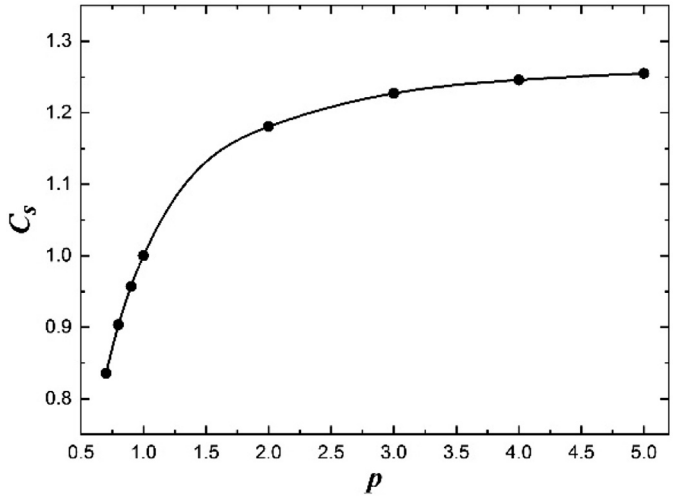

Fig. 3. The scaling coefficient C_s as a function of the surface shape parameter p for the superellipsoids defined in Eqs. (2) and (3).

We use both global and local order parameters to evaluate the degrees of different order forms. The global cubatic order parameter $I_{4,x}$, $I_{4,y}$, $I_{4,z}$ and S_4 are used to evaluate the global orientational order of the generated packings. Meanwhile, the normalized local cubatic order parameter $P_{4local,x}$, $P_{4local,y}$, $P_{4local,z}$, S_{4local}, and the normalized local bond-orientational order parameter Q_{6local} are used to evaluate the degrees of different local orientational and bond-orientational orders. The local order parameters reveal the average order degrees of the orientational and bond-orientational order corrections of each particle with a certain number of its nearest neighbor particles. Moreover, according to the Monte Carlo tests [30–32], the values of these local order parameters are in Gaussian distributions when the orientations or bond-orientations are randomly distributed. The means μ and standard deviations σ of the distributions are only related to the total particle amounts and the number of nearest neighbors taken into consideration. Therefore, the local order parameters are normalized by their corresponding means and standard deviations on the fully random state where the positions and orientations of particles are randomly distributed.

The values of the global orientational order parameters are in the range of [0,1] with 0 corresponding to the fully random packing and 1 corresponding to the ordered packing in which all the particles arrange along the same direction. The values of the normalized local order parameters describe the order-level distance of an actual packing to the fully random state. The values will be smaller if the packing is closer to the fully random state. The order constraint in the IMC method is $Op^{up} = 0.5$, which means that the distance of the generated packing to the fully random state is less than 0.5σ of the fully random state, making the final packing highly disordered. A more detailed description of these global and local order parameters can be found in Ref. [30–32, 34].

The normalized local bond-orientational and orientational order parameters are used as order constraints in the IMC method. For the z-dominant superellipsoids defined in Eq. (2), considering that these superellipsoids are axisymmetric and have only one principal axis, we use the normalized local cubatic order parameter $P_{4local,z}$ and the bond-orientational order parameter Q_{6local} in the IMC method to control the degrees of local order. For the y-dominant superellipsoids defined in Eq. (3), considering that these superellipsoids are not axisymmetric and their three main axes are not equivalent, besides the Q_{6local} which suppressing the bond-orientational order, we apply the normalized local cubatic order parameters $P_{4local,x}$, $P_{4local,y}$, $P_{4local,z}$ and S_{4local} to suppress the orientational orders in the x, y, z directions and their coupling orientational order, respectively. As can be seen in Figs. 4 and 5, the packing configurations generated via the IMC methods with the order constraints mentioned above are all highly disordered.

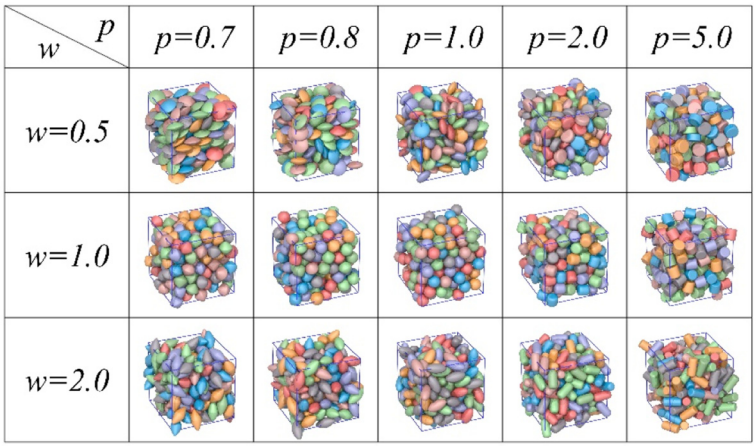

Fig. 4. The packing configurations of 200 *z*-dominant superellipsoids with different surface shape parameter *p* and natural aspect ratio *w*. All the packings are highly disordered.

3. Results and discussion

In this part, we investigate the aspect ratio effects and surface shape effects on the random packings of uniaxially variable superellipsoids, containing the *z*-dominant and *y*-dominant superellipsoids. Then we calculate the sphericities of the superellipsoids and carry out the Voronoi analysis for all the random packings we generate.

3.1. The z-dominant superellipsoids

Fig. 4 shows some typical packing configurations of the MDRPs of the *z*-dominant superellipsoids defined in Eq. (2) for various surface shape parameters *p* and aspect ratios *w*. All the packings are generated via the IMC method with the normalized local order parameters Q_{6local} and $P_{4local,z}$ served as order constraints. Meanwhile, we plot the global cubatic order parameter $I_{4,z}$, the normalized local cubatic order parameter $P_{4local,z}$, and the normalized local bond-orientational order parameter Q_{6local} for the MDRPs of *z*-dominant superellipsoids in Fig. 6. Although the values of the global cubatic order parameter $I_{4,z}$ near $w = 1.0$ are a little higher for larger surface shape parameter *p*, the values of $I_{4,z}$ are always smaller than 0.2, which is a very small value and demonstrates very few global orders. The $P_{4local,z}$ and Q_{6local} are all about 0.5 as a result of the small value of the order constraint $Op^{up} = 0.5$ in the IMC method. Therefore, all the packings we generate are highly disordered without obvious global or local ordered structures.

The random packing densities of the *z*-dominant superellipsoids are shown in Fig. 6(a), as functions of the natural aspect ratio *w* for different surface shape parameter *p*. The packing density curves are various for different surface shape parameter *p*. When the surface shape parameter *p* increases from 0.7 to 5.0, the packing density curve gradually changes from double-peaked to single-peaked and the locations of the peaks are not constant. Therefore, the aspect ratio effects on the random packing densities of *z*-dominant superellipsoids are not uniform under the natural aspect ratio *w* as results of the differences in surface shape. We note that when elongating or compressing the *z*-dominant superellipsoids defined in Eq. (2), both the two changing cross-sections (*xz* and *yz* cross-section) are superellipses with the shape parameter *p* and the natural aspect ratio *w*.

Then we redraw the packing density curve in Fig. 6(a) as a function of the effective aspect ratio R_z defined in section 2.2 for different surface shape parameter *p*, as shown in Fig. 7. Interestingly, when $p \le 1.0$, the packing density curves are "M" shaped with two peaks at $R_z \approx 0.7$, 1.5, and the maximal packing density at the two peaks are all about 0.72. Meanwhile, the local minimal packing density is always obtained at $R_z \approx 1.0$ and the minimal packing density decreases with the increase of the surface shape parameter *p*. Then when *p* increases from 1.0, the left peak moves to the bottom right and gradually vanishes, but the right peak still keep unchanged, located at $R_z \approx 1.5$ with the maximal packing density almost unchanged. Therefore, the maximal packing density for the *z*-dominant superellipsoids defined in Eq. (2) can always be obtained at $R_z \approx 1.5$ and are about 0.72, independent of the surface shape parameter *p*. Uniform shape elongation effects for the

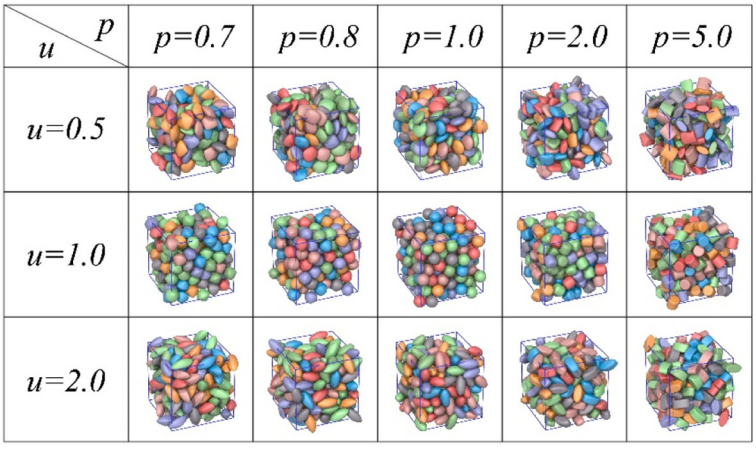

Fig. 5. The packing configurations of 200 *y*-dominant superellipsoids with different surface shape parameter *p* and natural aspect ratio *u*. All the packings are highly disordered.

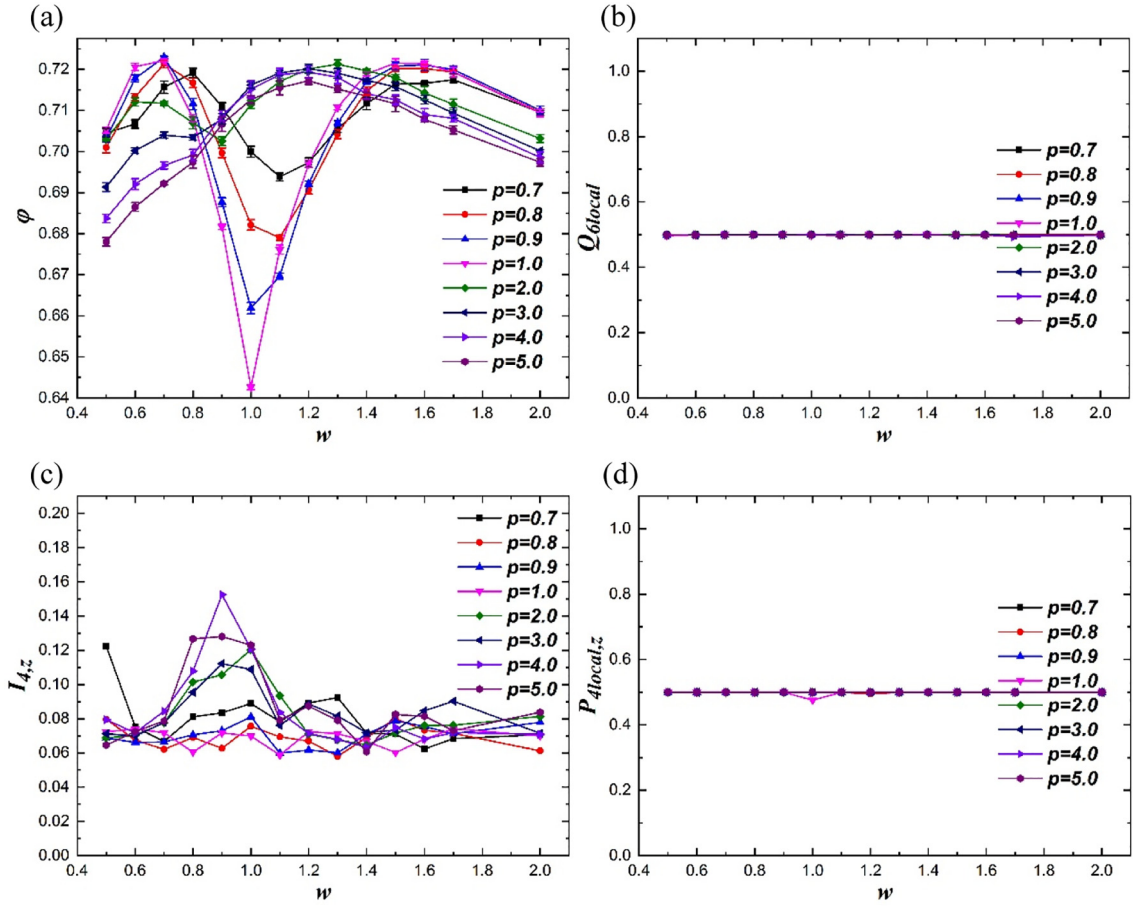

Fig. 6. The packing density φ (a), the normalized local bond-orientational order parameter Q_{6local} (b), the global cubatic order parameter $I_{4,z}$ (c), and the normalized local cubatic order parameter $P_{4local,z}$ (d) of the MDRPs for *z*-dominant superellipsoids defined in Eq. (2) as functions of the natural aspect ratio *w* for different surface shape parameter *p*.

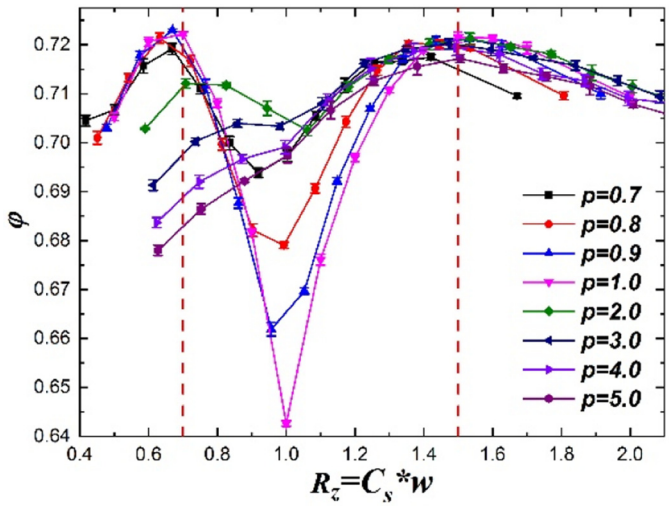

Fig. 7. The packing density φ of the MDRPs of *z*-dominant superellipsoids defined in Eq. (2) as a function of the effective aspect ratio R_z for different surface shape parameter *p*. The two red dashed lines are the aspect ratio value with $R_z = 0.7,1.5$. (For interpretation of the references to colour in this figure legend, the reader is referred to the web version of this article).

z-dominant superellipsoids are summarized as follows: the random packing density of the *z*-dominant superellipsoids is firstly improved when the effective aspect ratio increases from 1.0, then reaches the maximal value of about 0.72 when the effective aspect ratio is about 1.5, and finally decreases when the effective aspect ratio is further increasing. The aspect ratio effects are scaled to be uniform via the scaling coefficient C_s in Eq. (10), which is determined by the surface shape parameter *p* of the z-dominant superellipsoids, as shown in Fig. 3.

3.2. The *y*-dominant superellipsoids

We further investigate the aspect ratio effects for the *y*-dominant superellipsoids defined in Eq. (3). For these superellipsoids, the effective aspect ratio R_y is always equal to the natural aspect ratio *u*, regardless of the values of surface shape parameters *p*. Therefore, we use *u* to represent the aspect ratio. The MDRPs of *y*-dominant superellipsoids are generated via the IMC method as well. As mentioned in section 2.3, the *y*-dominant superellipsoids are not axisymmetric and their three main axes are not equivalent. Therefore, we use the normalized local order parameters $P_{4local,x}$, $P_{4local,y}$, $P_{4local,z}$, S_{4local} and Q_{6local} to fully suppress different order forms that can appear in the packings.

Some typical packing configurations of the MDRPs for the *y*-dominant superellipsoids defined in Eq. (3) are shown in Fig. 5. All the order parameters and the packing densities are drawn in Fig. 8, as functions of the natural aspect ratio *u* for different surface shape parameters *p*. As can be seen in Fig. 8, the constrained local order parameters $P_{4local,x}$, $P_{4local,y}$, $P_{4local,z}$, S_{4local} and Q_{6local} approach 0.5, and the global order parameters $I_{4,x}$, $I_{4,y}$, $I_{4,z}$ and S_4 are smaller than 0.2, as a result of the small value of order constraint $Op^{up} = 0.5$. Therefore, the order is successfully suppressed during the formation of the packing configurations and the final packings we generate are highly disordered as well.

Fig. 8(a) shows the aspect ratio effects on the packing densities of the MDRPs for the *y*-dominant superellipsoids with different surface

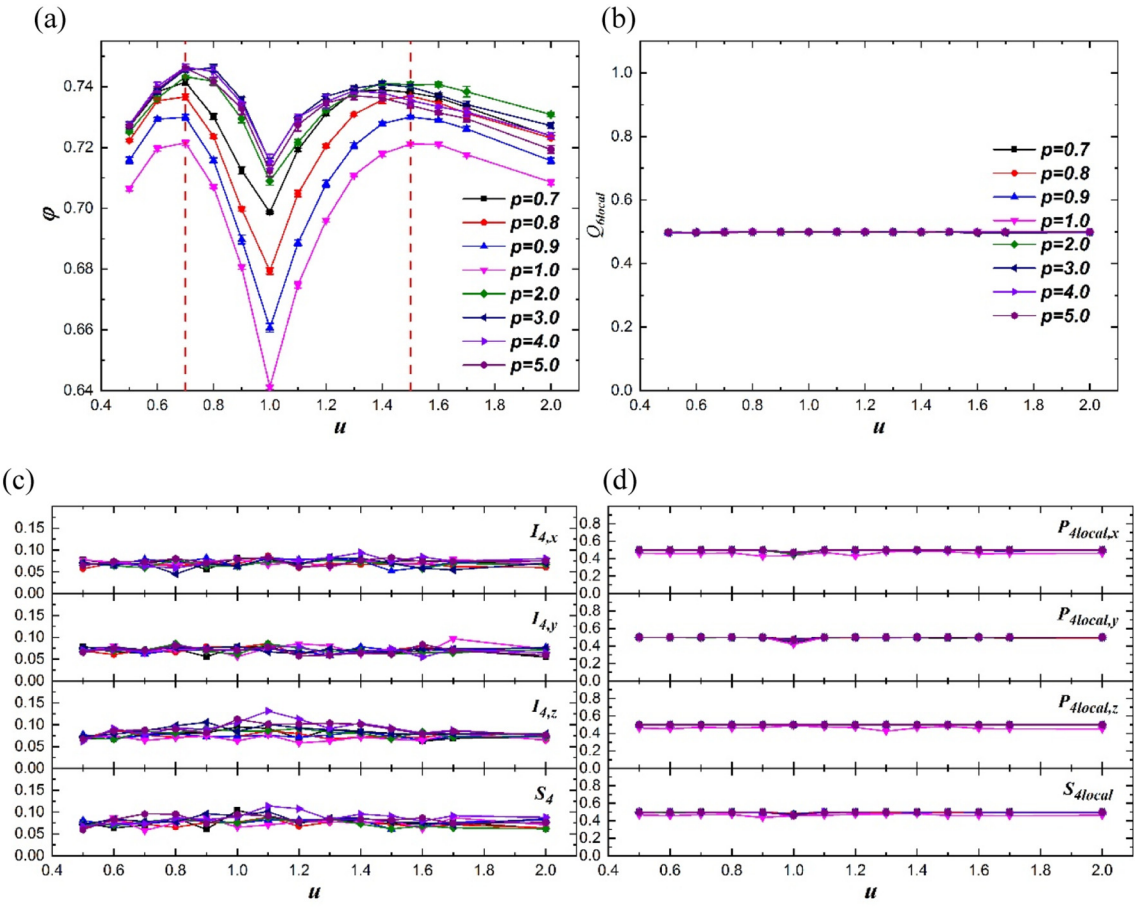

Fig. 8. The packing density φ (a), the normalized local bond-orientational order parameter Q_{6local} (b), the global cubatic order parameter $I_{4,x}$, $I_{4,y}$, $I_{4,z}$, S_4 (c), and the normalized local cubatic order parameter $P_{4local,x}$, $P_{4local,y}$, $P_{4local,z}$, S_{4local} (d) of the MDRPs for *y*-dominant superellipsoids defined in Eq. (3) as functions of the natural aspect ratio u for different surface shape parameter p. The two red dashed lines in (a) are the aspect ratio value with $u = 0.7,1.5$. (For interpretation of the references to colour in this figure legend, the reader is referred to the web version of this article).

shape parameter p. Rather different from the *z*-dominant superellipsoids, all the packing density curves for the *y*-dominant superellipsoids are in "M" shape with two maximums at $u \approx 0.7$, 1.5 and the minimum at $u = 1.0$, regardless of the surface shape parameter p. We note that when elongating or compressing the *y*-dominant superellipsoids defined in Eq. (3), the changing cross-sections are an ellipse (*xy* cross-section) and a superellipse (*yz* cross-section) with shape parameter p. Both the natural aspect ratio values of the ellipse and the superellipse are u.

Therefore, we conclude that for all the rod-like superellipsoids studied in this work, containing the *z*-dominant and *y*-dominant superellipsoids, uniform shape elongation effects are observed with the maximum located at about 1.5, if the effective aspect ratio is used. For the *y*-dominant superellipsoids, at least one cross-section of which is changing from a disk to an ellipse, uniform shape elongation and compression effects are observed with the packing density curve to be "M" shaped and the locations of local extremums to be identical.

We also note that the left peak in Fig. 8(a) is always no lower than the right peak for different surface shape parameters p. The maximal packing density of MDRPs for all the *y*-dominant superellipsoids we study is about 0.746 with the aspect ratio $w = 1.0$, $u = 0.7$, and the surface shape parameter $p = 5.0$. This value is larger than 0.72, which is the maximal random packing density for all the *z*-dominant superellipsoids. This value is also larger than 0.7405, which is the packing density of the densest mono-sized sphere packings. As shown in Fig. 9(b), this kind of particle is compressed from a rounded cylinder of Fig. 9(a), of which the *xy* and *yz* cross-sections are an ellipse and almost a rectangle, respectively, with the aspect ratio to be 0.7. The corresponding packing configuration is shown in Fig. 9(c). Therefore, a more effective way to improve the random packing density for non-spherical particles is to compress the particles along the non-symmetric axis.

3.3. The surface shape effects

In this work, we also study the surface shape effects on the packing densities of all the superellipsoids we concern. As shown in Fig. 10, the packing densities are drawn as functions of the surface shape parameter p for the *z*-dominant and *y*-dominant superellipsoids with different natural aspect ratios. However, no universal properties are observed among all the packing density curves. For the *z*-dominant superellipsoids, the packing density at $p = 1.0$ is not always the local minimum for all the packing density curves with different natural aspect ratios w. For $w = 0.7$ and 1.5, the packing density at $p = 1.0$ is even the local maximum. As for the *y*-dominant superellipsoids, the packing density at $p = 1.0$ is always the local minimum for all the packing density curves with different natural aspect ratios u. However, the locations of the maximums are not uniform for both the *z*-dominant and *y*-dominant superellipsoids.

In Fig. 11, we draw the packing density map as functions of both the effective aspect ratio and the surface shape parameter. The packing density of spheres ($p = 1.0$, $R_z = w = 1.0$, $R_y = u = 1.0$) is always a local minimum on the packing density map, which is consistent with the Ulam's conjecture [54] for random packings. Meanwhile, three and four high-density regions are observed in Fig. 11(a) and (b), respectively. The value of the effective aspect ratio for these high-density regions are all near 0.7 or 1.5, which shows uniform shape elongation

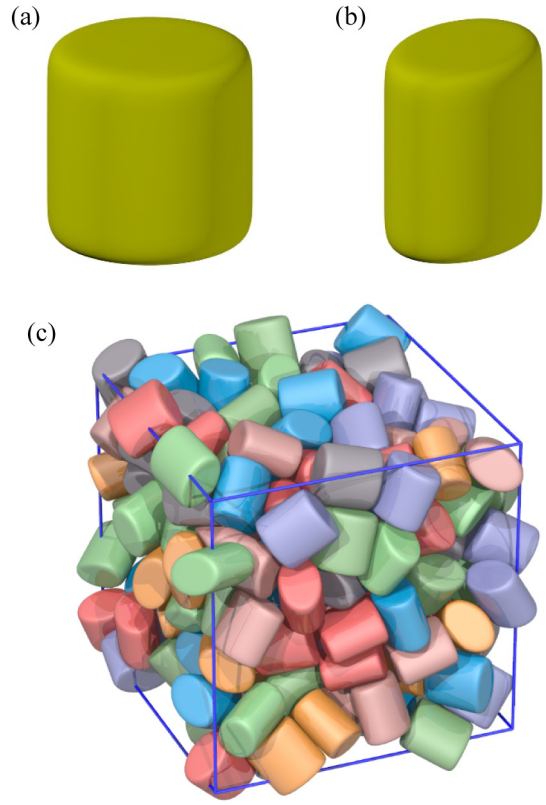

Fig. 9. (a) The superellipsoid with $w = 1.0$, $u = 1.0$, and $p = 5.0$. (b) The superellipsoid with $w = 1.0$, $u = 0.7$, and $p = 5.0$. (c) The packing configuration which corresponds to the highest packing density of 0.746.

effects for all the superellipsoids we concern. However, the value of the surface shape parameter p for these high-density regions are not identical. For the z-dominant superellipsoids, the high-density regions are closed in the p direction with $p \approx 1.0, 2.5$, but no high-density region is observed on the top left corner in Fig. 11(a). As for the y-dominant superellipsoids, the four high-density regions are symmetric in both R_y and p direction, but are not closed in the p direction. Both the regions with $R_y = 1.0$ and $p = 1.0$ are always the valleys on the packing density map in Fig. 11(b). We also note that the left high-density region in Fig. 11(b) extends along the p direction with considerably higher densities, meaning that the aspect ratio $R_y = 0.7$ is a more efficient value for improving the packing density and is valid for a wider value range of the surface parameter p.

In summary, uniform aspect ratio effects on the packing density are observed for the superellipsoids we concern about in this work. However, the surface shape effects are not universal if we just use the original surface shape parameter p. We also note that the surface shape parameter p is only applicable for the superellipsoids and is not a universal parameter that describes the surface shape. We use the sphericity to describe the surface shape in the next section.

3.4. The sphericities

The sphericity, which is defined as the ratio of the surface area of a sphere that has the same volume as the given particle to the surface area of that particle, is a commonly used shape parameter and is applicable to any particle shape [55,56]. The sphericity ψ can be defined as

$$\psi = \frac{\pi^{\frac{1}{3}}(6V_p)^{\frac{2}{3}}}{S_p}, \tag{11}$$

where V_p and S_p are the volume and surface area of a particle, respectively. As for the superellipsoids defined in Eq. (1), the volume V_p is calculated accurately with

$$V_p = \frac{2abc\Gamma\left(\frac{1}{2p_0}\right)\Gamma\left(\frac{1}{2p_0}\right)\Gamma\left(\frac{1}{2p_1}\right)\Gamma\left(\frac{1}{p_1}\right)}{3p_0p_1\Gamma\left(\frac{1}{p_0}\right)\Gamma\left(\frac{3}{2p_1}\right)}, \tag{12}$$

where $\Gamma(x) = \int_0^{+\infty} t^{x-1}e^{-t}dt$, $(x > 0)$ is the Gamma function, whose value can be directly obtained. However, the surface area S_p of the superellipsoids cannot be directly calculated and we use the numerical integration to obtain the values of S_p. We also note that only the surface areas of superellipsoids with the surface shape parameter $p \le 2.5$ are obtained with the relative error smaller than 0.003. The integration for larger values of p is difficult to be convergent with infinitesimal space step. Moreover, the relative errors of the S_p for superellipsoids with $p \le 1.4$ are smaller than 0.0001.

Fig. 12 shows the sphericities of the z-dominant and y-dominant superellipsoids studied in this work. As can be seen in Fig. 12(a) and (b), the maximal sphericity is not always obtained with the natural aspect ratio w or u to be 1.0 for different surface shape parameter p. When $p = 0.7, 0.8$ for the z-dominant superellipsoids, the maximal sphericity is obtained at $w = 1.1$. When $p = 0.7$ for the y-dominant superellipsoids, the maximal sphericity is obtained at $w = 0.9$.

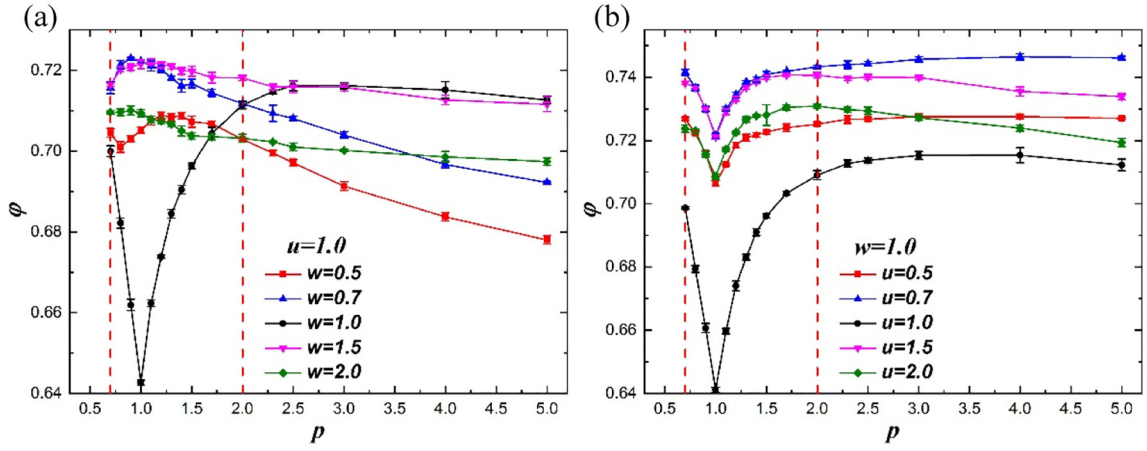

Fig. 10. (a) The packing density φ of the MDRPs for the z-dominant superellipsoids as functions of the surface shape parameter p for different natural aspect ratio w. (b) The packing density φ of the MDRPs for the y-dominant superellipsoids as functions of the surface shape parameter p for different natural aspect ratio u. The two red lines are the surface shape parameter value with $p = 0.7,2.0$. (For interpretation of the references to colour in this figure legend, the reader is referred to the web version of this article).

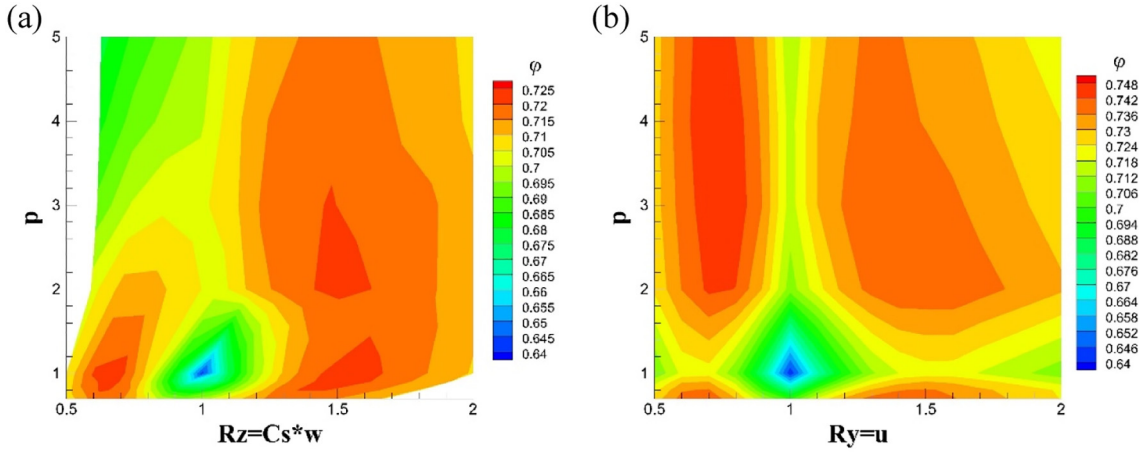

Fig. 11. The packing density map for the *z*-dominant (a) and *y*-dominant (b) superellipsoids as functions of both the effective aspect ratio and the surface shape parameter.

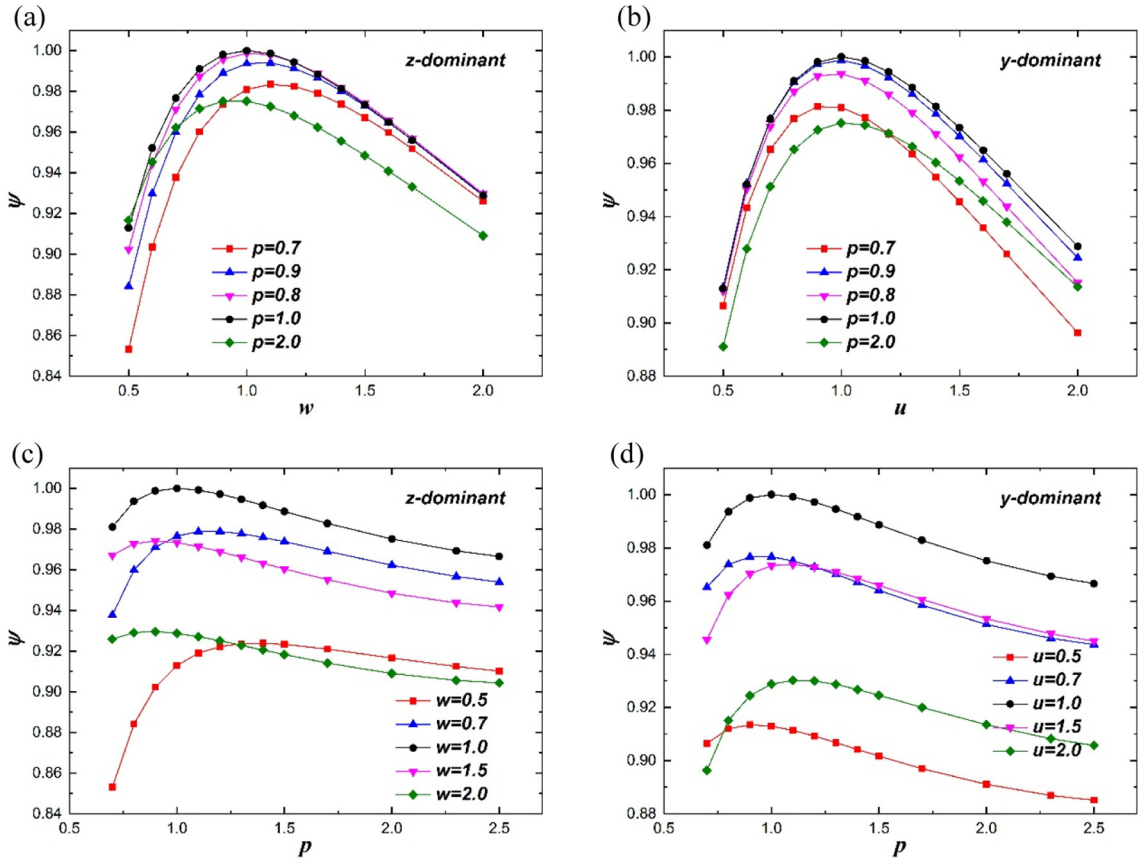

Fig. 12. The sphericities of the *z*-dominant (a, c) and *y*-dominant (b, d) superellipsoids as functions of the natural aspect ratio (a, b) and the surface shape parameter (c, d), respectively.

Meanwhile, the maximal sphericity is also not always obtained with the surface shape parameter $p = 1.0$ for different natural aspect ratio w or u, as shown in Fig. 12(c) and (d). In Fig. 12(c), when the natural aspect ratio $w = 0.5,0.7,1.0,1.5,2.0$ for the *z*-dominant superellipsoids, the maximal sphericity is obtained at $p = 1.4$, 1.2, 1.0, 0.9, 0.9, respectively. In Fig. 12(d), when the natural aspect ratio $u = 0.5,0.7,1.0,1.5,2.0$ for the *y*-dominant superellipsoids, the maximal sphericity is obtained at $p = 0.9$, 1.0, 1.0, 1.1, 1.1, respectively.

We redraw the packing density curves in Figs. 7, 8(a), 10(a) and (b), as functions of the sphericity ψ. As can be seen in Fig. 13(a), the elongating part with $R_z \geq 1.0$ and the compressing part with $R_z \leq 1.0$ of the $\varphi - \psi$ curve with $p \leq 1.0$ is uniform, which means that the "M" shaped packing density curve $\varphi - R_z$ is folded into a single-peaked curve $\varphi - \psi$ with the abscissa changed from R_z into ψ. Similar phenomena are also observed in Fig. 13(b) for the *y*-dominant superellipsoids with $p = 0.7$, 0.8, 0.9, 1.0, 2.0. We also note that the "M" shaped $\varphi - R$ curves are symmetric with two equal local maximums for the *y*-dominant superellipsoids with $p = 0.7$, 0.8, 0.9, 1.0, 2.0 and the *z*-dominant superellipsoids with $p = 0.7$, 0.8, 0.9, 1.0, as can be seen in Fig. 7 and Fig. 8(a). However, the elongating and compressing parts of the $\varphi - \psi$ curve are not uniform for the *z*-dominant superellipsoids

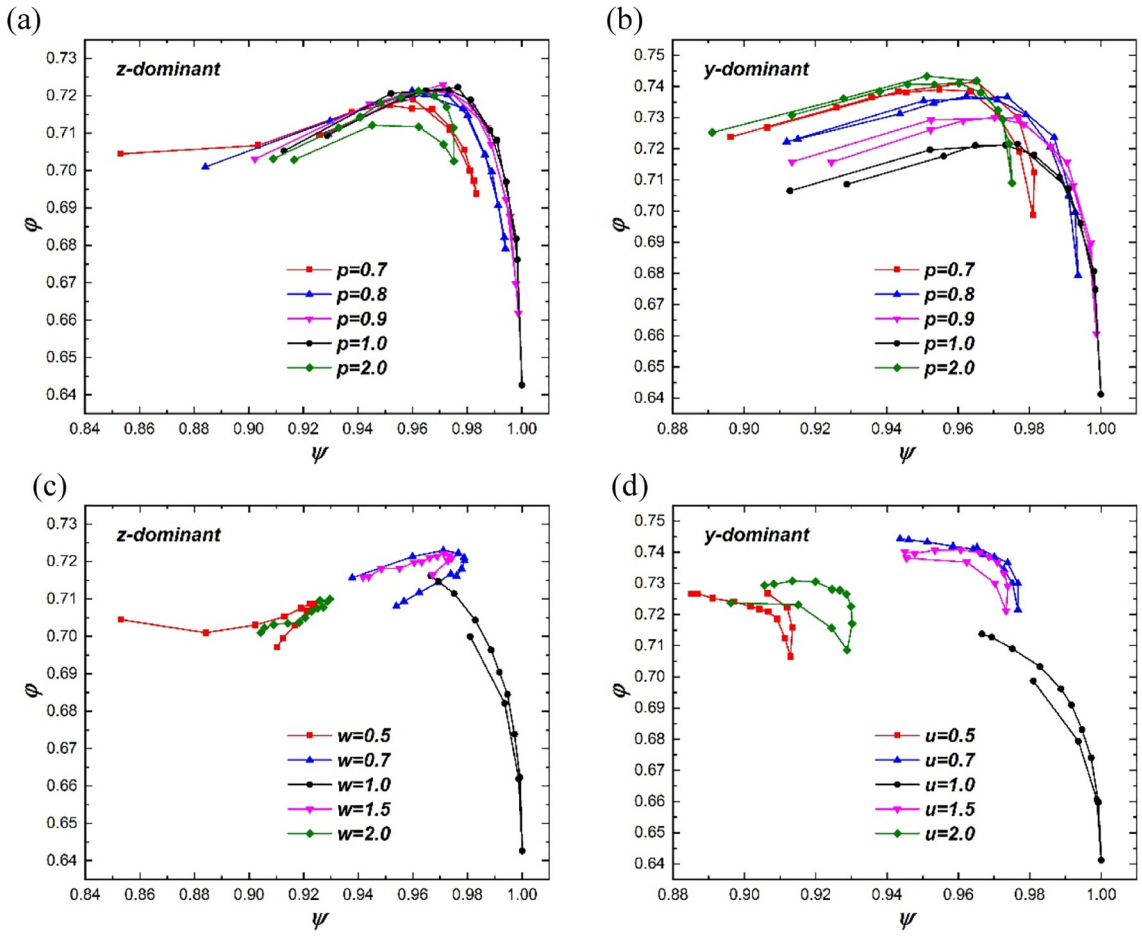

Fig. 13. The packing densities φ of the MDRPs we generate as functions of the sphericity ψ for the z-dominant (a, c) and y-dominant (b, d) superellipsoids. The points are classified by the surface shape parameter in (a, b) and the natural aspect ratio in (c, d), respectively. Meanwhile, the points are lined with the increase of the natural aspect ratio in (a, b) and the surface shape parameter in (c, d), respectively.

with $p = 2.0$, whose $\varphi - R$ curve is "M" shaped but the two local maximums are not equal. Finally, as can be shown in Fig. 13(c) and (d), no uniform phenomenon is observed on the $\varphi - \psi$ curves which are drawn from the $\varphi - p$ curves with different natural aspect ratio w or u.

Therefore, the compressing and elongating aspect ratio effects on the random packing density are equivalent if they have the same sphericity for the z-dominant and y-dominant superellipsoids whose $\varphi - R$ curves are "M" shaped with two equal local maximums. No more general surface shape effect on the random packing density is obtained if we use the sphericity as a shape parameter. A uniform surface shape parameter is required to describe the surface shape information of not only superellipsoids but also other shaped particles. More work will be carried out to find this surface shape parameter in the future.

3.5. The Voronoi analysis

The Voronoi diagram is often used to analyze the local packing properties of non-spherical random packings [11,30,32,41,57]. The values of the reduced local Voronoi cell volume $V_{local} = V_{cell}/V_p$ in the random packings are often in normal or log-normal distributions. Here, the V_p and V_{cell} are the volumes of the particle and its corresponding Voronoi cell, respectively. Moreover, linear (or exponential) relationships are observed between the mean and standard deviation of the values of V_{local} (or its reciprocal) for the random packings of ellipsoids [11,41], cylinders [32,41] and superellipsoids [30], regardless of their aspect ratios. In this work, we also tessellate the MDRPs of the uniaxially variable superellipsoids via the set Voronoi diagram method [58]. The surface of each superellipsoid in the packing is discretized into 2246 points, as a compromise between accuracy and computational cost [30]. Then the Voro++ program [59] is used to compute the Voronoi cell volumes for all the discrete points in a packing configuration. Finally, the Voronoi cell volume of a particle is calculated as the summation of the volumes of all its discrete points.

Fig. 14 shows the relationship between the mean V^{μ}_{local} and standard deviation V^{σ}_{local} of V_{local} for the MDRPs of the z-dominant and y-dominant superellipsoids. As shown in Fig. 14(a) and (b), the $V^{\sigma}_{local} - V^{\mu}_{local}$ points are obtained from the packing configurations in Fig. 6 and Fig. 8 and are classified by the value of surface shape parameter p. Two linear relationships are observed in both figures. When p is smaller than 2.0, a common and clear linear relationship between V^{σ}_{local} and V^{μ}_{local} is observed. However, when p is even larger, the $V^{\sigma}_{local} - V^{\mu}_{local}$ points keep away from the common line and form another much rougher common line. Moreover, the $V^{\sigma}_{local} - V^{\mu}_{local}$ relationships for the z-dominant and y-dominant superellipsoids are very similar to those for the superellipsoids which are elongated or compressed superballs in Ref. 30, demonstrating general local packing properties for all the superellipsoids defined in Eq. (1).

In Fig. 14(c) and (d), we also plot the $V^{\sigma}_{local} - V^{\mu}_{local}$ points obtained from the packing configurations in Fig. 10. The points are now classified by the value of the natural aspect ratio. No common linear relationship is observed for the superellipsoids with the same natural aspect ratio. Therefore, when compressing or elongating a superellipsoid with the surface shape unchanged, the mean and standard deviation of the reduced local Voronoi cell volumes V_{local} in the random packing will

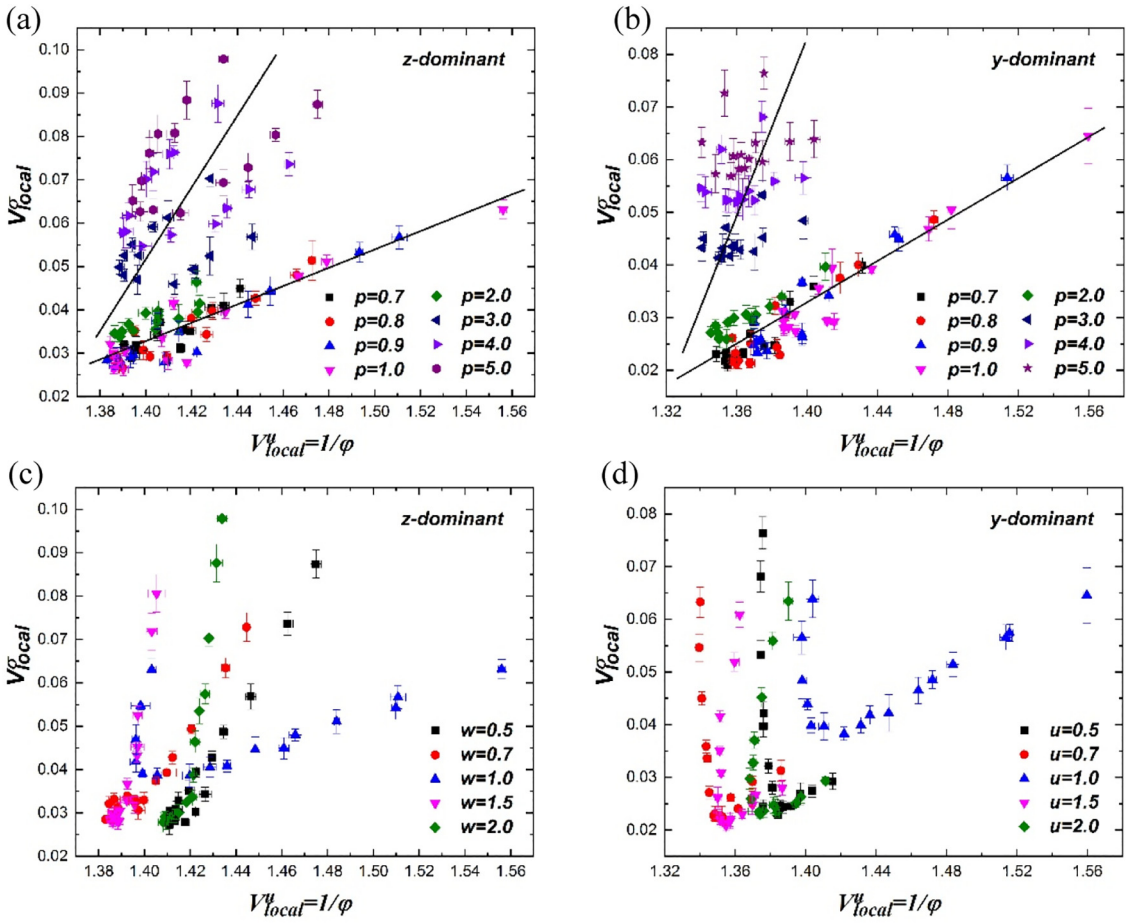

Fig. 14. The relationship between the mean V^{μ}_{local} and standard deviation V^{σ}_{local} of the local Voronoi cell volume V_{local} for the MDRPs of the *z*-dominant (a, c) and *y*-dominant (b, d) superellipsoids. The points are classified by the surface shape parameter in (a, b) and the natural aspect ratio in (c, d), respectively.

vary linearly. However, when changing the surface shape of a superellipsoid with the aspect ratio unchanged, the mean and standard deviation will vary in a non-universal way. The surface shape of particles plays a more important role in changing the local packing properties than the aspect ratio.

4. Conclusions

We obtain the MDRPs of uniaxially variable superellipsoids elongated in different axial directions, axisymmetric or not axisymmetric, via the IMC method. All the packing configurations we generate are highly disordered, as evaluated via different orientational and bond-orientational order parameters.

We propose new definitions of the aspect ratios along different axial directions, i.e. the effective aspect ratios R_y and R_z, which take the effects of particle surface shape into account. Uniform shape elongation effects on the random packing density are observed for all the uniaxially variable superellipsoids when the newly defined effective aspect ratios are applied. Both for the *z*-dominant and *y*-dominant superellipsoids, the packing density is firstly improved when the effective aspect ratio R increases from 1.0, then reaches the maximal value with $R \approx 1.5$ and finally decreases when R is further increased. Moreover, uniform shape elongation and compression effects are observed for the *y*-dominant superellipsoids. The packing density curves for the *y*-dominant superellipsoids are always in "M" shape for all the surface shape parameters with the maximums at $R_y \approx 0.7$, 1.5 and the minimum at $R_y = 1.0$.

Then we study the surface shape effects on the random packing density and no universal properties are observed among all the packing density curves as functions of the surface shape parameter p. We draw the packing density map as functions of both the effective aspect ratio and the surface shape parameter. Symmetric high-density regions are observed for both the *z*-dominant and *y*-dominant superellipsoids. The random packing density of spheres is always a local minimum. For the *z*-dominant superellipsoids, the high-density regions are closed in the p direction with $p \approx 1.0$, 2.5, but no high-density region is observed on the top left corner. As for the *y*-dominant superellipsoids, the four high-density regions are symmetric in both R_y and p direction, but are not closed in the p direction.

We also calculate the sphericities of the superellipsoids we study and find that the compressing and elongating aspect ratio effects on the random packing density are equivalent if they have the same sphericity for the superellipsoids with the $\varphi - R$ curve to be "M" shaped with two equal local maximums. Finally, we carry out the Voronoi analysis for all the random packings we generate. Rough linear relationships between the mean and standard deviation of the reduced local Voronoi cell volumes are observed when the points are classified by the surface shape parameter, demonstrating that the surface shape of particles plays a more important role in changing the local packing properties than the aspect ratio.

Our work provides a uniform definition for the aspect ratio, which incorporates curvature information and reveals hidden universal packing characteristics, leading to a better understanding towards the particle shape effects on random packings. We also note that the new definition for aspect ratio is only applicable for superellipsoids and its limiting cases (cubes, octahedra and cylinders), which have three orthogonal symmetry planes, and is based on the areas of the three symmetry planes. However, for general polyhedra without three orthogonal symmetry planes, such as tetrahedra and prisms with

unequal cross-sections, the new defined aspect ratio based on the areas of the cross-sections is not applicable. More complicated surface information should be captured via a more general shape metric. A more general definition of the aspect ratio for differently shaped particles will be carried out in our future work. Moreover, the definition of uniform surface shape parameter and the biaxial aspect ratio effects on the packing densities of MDRPs will also be carried out in our future work.

Declaration of Competing Interest

The authors declare that they have no known competing financial interests or personal relationships that could have appeared to influence the work reported in this paper.

Acknowledgements

This work was supported by the National Natural Science Foundation of China (Grant No. 11572004 and 11972047), the China Postdoctoral Science Foundation (Grant No. 2019TQ0040) and the High-performance Computing Platform of Peking University.

References

[1] S. Torquato, F.H. Stillinger, Jammed hard-particle packings: from Kepler to Bernal and beyond, Rev. Mod. Phys. 82 (2010) 2633.
[2] A.J. Liu, S.R. Nagel, The jamming transition and the marginally jammed solid, Annu. Rev. Condens. Matter Phys. 1 (2010) 347–369.
[3] G. Parisi, F. Zamponi, Mean-field theory of hard sphere glasses and jamming, Rev. Mod. Phys. 82 (2010) 789–845.
[4] P.F. Damasceno, M. Engel, S.C. Glotzer, Predictive self-assembly of polyhedra into complex structures, Science 337 (2012) 453–457.
[5] G. Lu, J.R. Third, C.R. Müller, Discrete element models for non-spherical particle systems: from theoretical developments to applications, Chem. Eng. Sci. 127 (2015) 425–465.
[6] W. Zhong, A. Yu, X. Liu, Z. Tong, H. Zhang, DEM/CFD-DEM modelling of non-spherical particulate systems: theoretical developments and applications, Powder Technol. 302 (2016) 108–152.
[7] A. Baule, F. Morone, H.J. Herrmann, H.A. Makse, Edwards statistical mechanics for jammed granular matter, Rev. Mod. Phys. 90 (2018), 015006.
[8] S. Torquato, Perspective: basic understanding of condensed phases of matter via packing, J. Chem. Phys. 149 (2018), 020901.
[9] M. Clusel, E.I. Corwin, A.O.N. Siemens, J. Brujic, A 'granocentric' model for random packing of jammed emulsions, Nature 460 (2009) 611–615.
[10] J. Tian, Y. Xu, Y. Jiao, S. Torquato, A geometric-structure theory for maximally random jammed packings, Sci. Rep. 5 (2015) 16722.
[11] F.M. Schaller, M. Neudecker, M. Saadatfar, G.W. Delaney, G.E. Schröder-Turk, M. Schröter, Local origin of global contact numbers in frictional ellipsoid packings, Phys. Rev. Lett. 114 (2015) 158001.
[12] Y. Kallus, The random packing density of nearly spherical particles, Soft Matter 12 (2016) 4123–4128.
[13] C. Song, P. Wang, H.A. Makse, A phase diagram for jammed matter, Nature 453 (2008) 629–632.
[14] A. Donev, I. Cisse, D. Sachs, E.A. Variano, F.H. Stillinger, R. Connelly, S. Torquato, P.M. Chaikin, Improving the density of jammed disordered packings using ellipsoids, Science 303 (2004) 990–993.
[15] P.M. Chaikin, A. Donev, W. Man, F.H. Stillinger, S. Torquato, Some observations on the random packing of hard ellipsoids, Ind. Eng. Chem. Res. 45 (2006) 6960–6965.
[16] A. Donev, R. Connelly, F.H. Stillinger, S. Torquato, Underconstrained jammed packings of nonspherical hard particles: ellipses and ellipsoids, Phys. Rev. E 75 (2007), 051304.
[17] S. Wouterse, R. Williams, A.P. Philipse, Effect of particle shape on the density and microstructure of random packings, J. Phys. Condens. Mat. 19 (2007) 406215.
[18] S.R. Williams, A.P. Philipse, Random packings of spheres and spherocylinders simulated by mechanical contraction, Phys. Rev. E 67 (2003), 051301.
[19] R.A. Abreu, F.W. Tavares, M. Castier, Influence of particle shape on the packing and on the segregation of spherocylinders via Monte Carlo simulations, Powder Technol. 134 (2003) 167–180.
[20] X. Jia, M. Gan, Validation of a digital packing algorithm in predicting powder packing densities, Powder Technol. 174 (2007) 10–13.
[21] M. Bargiel, Geometrical Properties of Simulated Packings of Spherocylinders, Proceeding of 8th International Conference on Computational Science, 5102, Springer-Verlag, Berlin, 2008 126–135.
[22] P. Lu, S. Li, J. Zhao, L. Meng, A computational investigation on random packings of sphere-spherocylinder mixtures, Sci. China Phys. Mech. Astron. 53 (2010) 2284–2292.
[23] A.V. Kyrylyuk, M.A. van de Haar, L. Rossi, A. Wouterse, A.P. Philipse, Isochoric ideality in jammed random packings of non-spherical granular matter, Soft Matter 7 (2011) 1671–1674.
[24] J. Zhao, S. Li, R. Zou, A. Yu, Dense random packings of spherocylinders, Soft Matter 8 (2012) 1003–1009.
[25] F. Córdova, J.S.V. Duijneveldt, Random packing of hard spherocylinders, J. Chem. Eng. Data 59 (2014) 3055–3060.
[26] L. Meng, Y. Jiao, S. Li, Maximally dense random packings of spherocylinders, Powder Technol. 292 (2016) 176–185.
[27] G. Cinacchi, S. Torquato, Hard convex lens-shaped particles: metastable, glassy and jammed states, Soft Matter 14 (2018) 8205–8218.
[28] S. Faure, A. Lefebvre-Lepot, B. Semin, Dynamic numerical investigation of random packing for spherical and nonconvex particles, ESAIM: Proc. 28 (2009) 13–32.
[29] A. Baule, R. Mari, L. Bo, L. Portal, H.A. Makse, Mean-field theory of random close packings of axisymmetric particles, Nat. Commun. 4 (2013) 2194.
[30] L. Liu, Z. Yu, W. Jin, Y. Yuan, S. Li, Uniform and decoupled shape effects on the maximally dense random packings of hard superellipsoids, Powder Technol. 338 (2018) 67.
[31] L. Liu, Z. Li, Y. Jiao, S. Li, Maximally dense random packings of cubes and cuboids via a novel inverse packing method, Soft Matter 13 (2017) 748–757.
[32] L. Liu, Y. Yuan, W. Deng, S. Li, Evolutions of packing properties of perfect cylinders under densification and crystallization, J. Chem. Phys. 149 (2018) 104503.
[33] L. Liu, P. Lu, L. Meng, W. Jin, S. Li, Order metrics and order maps of octahedron packings, Phys. A 444 (2016) 870–882.
[34] L. Liu, S. Li, Shape effects on packing properties of bi-axial superellipsoids, Powder Technol. 364 (2020) 49–59.
[35] A.H. Barr, Superquadrics and angle-preserving transformations, IEEE Comput. Graph. Appl. 1 (1981) 11–23.
[36] R. Ni, A.P. Gantapara, J. de Graaf, R. van Roij, M. Dijkstra, Phase diagram of colloidal hard superballs: from cubes via spheres to octahedra, Soft Matter 8 (2012) 8826–8834.
[37] J.W. Perram, M. Wertheim, Statistical mechanics of hard ellipsoids. I. Overlap algorithm and the contact function, J. Comput. Phys. 58 (1985) 409–416.
[38] A. Donev, Jammed Packings of Hard Particles, Princeton University, 2006 PhD thesis.
[39] X. Jia, R. Caulkin, R.A. Williams, Z. Zhou, A. Yu, The role of geometric constraints in random packing of non-spherical particles, Europhys. Lett. 92 (2010) 68005.
[40] Z. Zhou, R. Zou, D. Pinson, A. Yu, Dynamic simulation of the packing of ellipsoidal particles, Ind. Eng. Chem. Res. 50 (2011) 9787–9798.
[41] K. Dong, C. Wang, A. Yu, Voronoi analysis of the packings of non-spherical particles, Chem. Eng. Sci. 153 (2016) 330–343.
[42] T.C. Hales, A proof of the Kepler conjecture, Ann. Math. 162 (2005) 1065–1185.
[43] A. Donev, F.H. Stillinger, P.M. Chaikin, S. Torquato, Unusually dense crystal packings of ellipsoids, Phys. Rev. Lett. 92 (2004) 255506.
[44] W. Jin, Y. Jiao, L. Liu, Y. Yuan, S. Li, Dense crystalline packings of ellipsoids, Phys. Rev. E 95 (2017), 033003.
[45] D. Frenkel, B.M. Mulder, J.P. Mctague, Phase diagram of a system of hard ellipsoids, Phys. Rev. Lett. 52 (1984) 287–290.
[46] P.J. Camp, C.P. Mason, M.P. Allen, The isotropic–nematic phase transition in uniaxial hard ellipsoid fluids: coexistence data and the approach to the Onsager limit, J. Chem. Phys. 105 (1996) 2837.
[47] G. Bautista-Carbajal, A. Moncho-Jordá, G. Odriozola, Further details on the phase diagram of hard ellipsoids of revolution, J. Chem. Phys. 138 (2013), 064501.
[48] P.J. Camp, M.P. Allen, Phase diagram of the hard biaxial ellipsoid fluid, J. Chem. Phys. 106 (1997) 6681.
[49] Y. Jiao, F.H. Stillinger, S. Torquato, Distinctive features arising in maximally random jammed packings of superballs, Phys. Rev. E 81 (2010), 041304.
[50] Y. Jiao, F.H. Stillinger, S. Torquato, Optimal packings of superballs, Phys. Rev. E 79 (2009), 041309.
[51] R.D. Batten, F.H. Stillinger, S. Torquato, Phase behavior of colloidal superballs: shape interpolation from spheres to cubes, Phys. Rev. E 81 (2010), 061105.
[52] G.W. Delaney, P.W. Cleary, The packing properties of superellipsoids, Europhys. Lett. 89 (2010) 34002.
[53] S. Zhao, N. Zhang, X. Zhou, L. Zhang, Particle shape effects on fabric of granular random packing, Powder Technol. 310 (2017) 175–186.
[54] Y. Jiao, S. Torquato, Maximally random jammed packings of platonic solids: Hyperuniform long-range correlations and isostaticity, Phys. Rev. E 84 (2011), 041309.
[55] H. Wadell, Volume, shape, and roundness of quartz particles, J. Geol. 43 (1935) 250–280.
[56] R. Zou, A. Yu, Evaluation of the packing characteristics of mono-sized non-spherical particles, Powder Technol. 88 (1996) 71–79.
[57] Y. Yuan, W. Deng, S. Li, Structural universality in disordered packings with size and shape polydispersity, Soft Matter 16 (2020) 4528–4539.
[58] F.M. Schaller, S.C. Kapfer, M.E. Evans, M.J.F. Hoffmann, T. Aste, M. Saadatfar, K. Mecke, G.W. Delaney, G.E. Schröder-Turk, Set Voronoi diagrams of 3D assemblies of aspherical particles, Philos. Mag. 93 (2013) 3993–4017.
[59] C.H. Rycroft, Voro++: a three-dimensional Voronoi cell library in C++, Chaos 19 (2009), 041111.